2022-08

Coastal dune dynamics in embayed settings with sea-level rise Examples from the exposed and macrotidal north coast of SW England

Masselink, Gerd
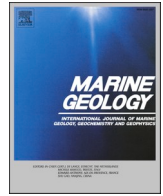
http://hdl.handle.net/10026.1/19734

Research Article

Coastal dune dynamics in embayed settings with sea-level rise – Examples from the exposed and macrotidal north coast of SW England

Gerd Masselink [a,*], Sue Brooks [b], Tim Poate [a], Christopher Stokes [a], Tim Scott [a]

[a] *Coastal Processes Research Group, University of Plymouth, PL4 8AA Plymouth, UK*
[b] *Department of Geography, Birkbeck University of London, WC1E 7HX London, UK*

A B S T R A C T

Coastal dune systems are natural forms of coastal defence, but are expected to exhibit increased erosion rates due to climate change impacts, notably sea-level rise and, potentially, increased storminess. This is especially the case in embayed coastal settings, i.e., where there are no significant sediment inputs into the beach/dune system from longshore sources. Dune development is closely linked to that of beaches that lie seaward, but their temporal dynamics tend to be asynchronous. So, whereas beaches are generally highly variable over a short- to medium-term (event–decadal) time scales, potentially obscuring a longer-term (decadal–centennial) sea-level signal, dunes display a low-pass filtered response which may contain a sea-level signal.

In this study, we investigate the decadal-scale, inter-annual dynamics of 25 embayed coastal dune systems along the exposed and macrotidal north coast of SW England. We then compare the observed behaviour with that hindcasted from simple parametric models and forecast future dune retreat rates due to sea-level rise. We show that practically all exposed dune systems show retreat with a regionally-averaged retreat rate of the dune foot of 0.5 m yr^{-1}. The majority of retreat occurred over a small number of especially energetic winters and it was found that dune retreat is not automatically linked to dune volumetric change. Many of the retreating dune systems display so called 'dune roll-over', characterised by removal of sediment from the dune face and deposition at the dune top. Observed dune retreat rates were 2–3 times larger than predicted using simple parametric retreat models forced by sea-level rise. This suggests that the retreat models are inappropriate and/or that sea-level rise in itself may be insufficient to explain the observed retreat and that increased winter storminess may be implicated.

A key factor in driving dune retreat is considered to be the number of hours that waves reach the dune foot or the excess runup energy present at the dune foot elevation. Both sea-level rise and enhanced storminess will increase exposure of the dune foot to energetic wave action and this is expected to accelerate dune retreat rates in these settings. Application of parametric shoreline retreat models that account for the acceleration in rate of sea-level rise predicts c. 40 m of dune retreat by 2100 with a considerable range in retreat (20–75 m), resulting from uncertainty in model choice and parameterisation. Simply extrapolating the current dune retreat rate also results in c. 40 m of dune retreat by 2100, but this approach ignores the potential acceleration in dune retreat rate due to an increase in the rate of sea-level rise.

The combination of analysis of multi-annual coastal dune morphological change along with application of dune retreat models can provide useful insights into future dune evolution for coastal planners and managers.

1. Introduction

Dune systems are present along many low-lying coastlines and are often the first line of defence against the impacts of storms (Den Heijer et al., 2012). The dune, foredune and beach are highly dynamic with complex responses to storms depending on the interaction between waves, wind and vegetation (Ruessink et al., 2019). According to Sallenger (2000), the main impact from storms arises from the difference between the elevation of the dune base and the water level (tide + storm surge + wave run-up) as this controls the occurrence and duration of the wetting of the dune base. When dunes are scarped during storms, sediment is deposited on the beach and in nearshore region (Wernette et al.,

2016). Subsequently, nearshore bars may migrate onshore and return sediment to the beach, which becomes wider and higher, until sediment can be displaced by aeolian processes to form embryo dunes and/or contribute to foredune development (Jackson et al., 2016; Brooks et al., 2017; Crapoulet et al., 2017; Guisado-Pintado and Jackson, 2019).

Cross-shore sediment exchange between beach and dune has been captured by high resolution (spatial and temporal) ground survey campaigns. These have shown how beach levels vary considerably over short term timescales in response to storms (Coco et al., 2014; Masselink et al., 2016a; Turner et al., 2016; Castelle et al., 2020), with recovery taking place as mobile sediment is returned to the inter-tidal and supra-tidal beach (Vousdoukas et al., 2012; Backstrom et al., 2015; Scott et al., 2016; Burvingt et al., 2018; Konstantinou et al., 2021). Although storm-induced dune scarping takes place over hours or days, it can take years or decades for sediment to build dunes back to pre-storm elevations and morphologies (Houser et al., 2015). Being able to predict dune resilience in the face of rising sea levels (IPCC, 2021) and changing storminess (Knutson et al., 2021) requires an understanding of past and present dune responses, as well as their recovery rates.

Extreme water levels and storm forcing can arise from individual storms aligning with high spring tides and surges (Spencer et al., 2015; Masselink et al., 2016b; Guisado-Pintado and Jackson, 2019), or from clusters of storms delivering multi-phases of extreme water levels and wave activity (Ferreira, 2006; Dissanayake et al., 2015). The Atlantic west coast of Europe is especially vulnerable to extra-tropical storms (Lozano et al., 2004) as has been amply demonstrated by the impacts of the 2013/14 winter extreme storminess (Castelle et al., 2015; Kandrot et al., 2016; Masselink et al., 2016b). The dune base, separating the wave-dominated beach from the wind-dominated dune, is considered especially vulnerable to extreme water levels and wave conditions with exposure to energetic wave runup resulting in dune scarping and retreat.

Shoreline change analysis is a rapidly-evolving research field driven by advances in data acquisition, analysis and visualisation (Pollard et al., 2019; Rogers et al., 2021). An ability to analyse past shoreline change within the context of known sea-level rise underpins current understanding of shoreline responses, and also informs likely future responses (Brooks and Spencer, 2012). Using available data sets we can extract either datum-based (e.g., from LiDAR) or proxy-based (e.g., from aerial photographs or satellites) shorelines (Carapuço et al., 2016) with different processes and scales of change captured by these different metrics (Pollard et al., 2020). Available data for shoreline change analysis have varying spatial and temporal resolution. In general, data sets with high spatial resolution (e.g., LiDAR) tend to be temporally low resolution, while high temporal resolution (e.g., satellite imagery) combines with reduced spatial resolution (Vos et al., 2019). It is vital that datasets cover a sufficient timeframe to overcome noise from wave forcing and other factors driving coastal change, such that the sea-level rise signal can be detected (Vitousek et al., 2017; Mccarroll et al., 2021); the so-called 'time to emergence' issue (Ponte et al., 2019). Multi-annual to decadal-scale oscillations are frequently observed in coastal dynamics in relation to variations in atmospheric forcing and storm generation (Burningham and French, 2013; Brooks and Spencer, 2014; Masselink et al., 2016b; Loureiro and Cooper, 2019), which hinders the detection of sea-level rise induced shoreline change. Further, recent research from tide gauge analysis has demonstrated that sea level can vary by as much as 0.3 m in relation to the 18.6 year nodal cycle (Peng et al., 2019). It is only now that datasets are beginning to emerge that cover multi-decadal timescales at an acceptable spatial resolution to have confidence in the resulting analysis. LiDAR is becoming widely used in shoreline change analysis, as exemplified by the work of Doyle and Woodroffe (2018) for dunes in NSW, Australia.

This paper addresses dune dynamics along the north coast of SW England and future dune development under ongoing sea-level rise using a combination of topographic survey and LiDAR data, dune foot wave exposure modelling and application of simple retreat models forced by sea-level rise. In addition to characterising the spatial variability in dune dynamics along this highly variable coastal region, our key premise is that investigation of the dune foot will provide potentially the 'cleanest' sea-level rise signal, i.e., least affected by the considerable multi-annual and decadal variability that may obscure any sea-level trend in the beach morphology. The key objectives of this paper are to: (1) provide a regional overview of coastal dune dynamics along the embayed, exposed and macrotidal coast of north Cornwall; and (2) compare the observed dune behaviour with that hindcasted from simple parametric models and forecast future dune retreat rates due to sea-level rise. To begin with, we consider decadal-scale coastal change using available data sets going back to 2006. We focus on identifying the elevation threshold where clear changes in morphological response occur, from highly variable noisy responses to smoother and more gradual changes. We then combine a 40-year time series of wave height and water level (with and without the sea-level rise component) to investigate the frequency with which elevation thresholds are reached. The Bruun Rule (Bruun, 1954) and its modification to account for onshore sediment transport (Rosati et al., 2013), as well as a recently proposed approach for specifically addresses dune retreat as a result of sea-level rise (Davidson-Arnott and Bauer, 2021), are then used to hindcast the current dune retreat rate and forecast future dune retreat.

2. Geographic setting

All dune systems presented in this paper are located on the north coast of the southwest England (Fig. 1). The coastline is exposed to large wind and swell-dominated conditions arriving from the west (280°; Fig. 1) with distinct seasonal variability in significant wave height, with averages from $H_s = 1.4$ m in summer to $H_s = 2.2$ m in winter, and with extreme storm waves exceeding $H_s = 6$ m (Masselink et al., 2016b). The macrotidal regime increases to the north with spring tide ranges from 5.4 m at Sennen in the south to 8.3 m at Croyde in the north. Using wind data from Perranporth, the prevailing wind direction is west-southwest (260°) with the dominant weather systems arriving from the Atlantic and tracking east across SW England. The mean wind speed in the summer months is 5.7 m s^{-1} while the winter average is 8.2 m s^{-1} (Fig. 1).

The region is made up of varied geological composition, from hardwearing igneous extrusions to softer sedimentary beds (Scott et al., 2011), resulting in a predominantly embayed coastline (King et al., 2021) of cliffs and sandy beaches dominated by cross-shore sediment transport due to the wave exposure. A wide variety in dune systems are presented in terms of setting, size and morphology (Fig. 2). Excluding the large embayment of St Ives Bay (Porthkidney, Gwithian and Godrevy), the dune-backed embayments average 0.7 km alongshore and 120 m cross-shore from high water to dune crest, and each embayment has a backshore dune system which varies in spatial extent and elevation. The largest dune systems are situated in the larger bays, including Woolacombe, Saunton, Widemouth Bay, Constantine, Fistral, Crantock, Penhale, Perranporth, Gwithian and Sennen (Table 1; Fig. 1; Fig. 2). There are also a number of smaller active dunes located in the narrower embayments (e.g., Poly Joke, Treyarnon, Porthcothan, Mawgan Porth and Porthtowan). Many dune systems in the study area are so called 'climbing dunes', where the dunes are underlain by bedrock, rather than coastal plain deposits. This means that the maximum dune elevations do not necessarily correspond to the thickness of the dune deposit. Most dunes are also characterised by an erosive front and accretionary foredunes are generally absent (Fig. 3a), suggesting that sediment supply to these dune systems is limited.

Three of the sites are located within the mouth of the Camel Estuary, offering more sheltered conditions from the predominant southwesterly wave events (Daymer Bay, Rock Beach and Harbour Cove; Fig. 2). Of these, only the Harbour Cove dune system has a prograding foredune (Fig. 3b). While the majority of dune systems are 'active', some have been built-over and/or are adjacent coastal infrastructure, restricting growth and capacity to transition (e.g., Porthtowan and Porthcothan).
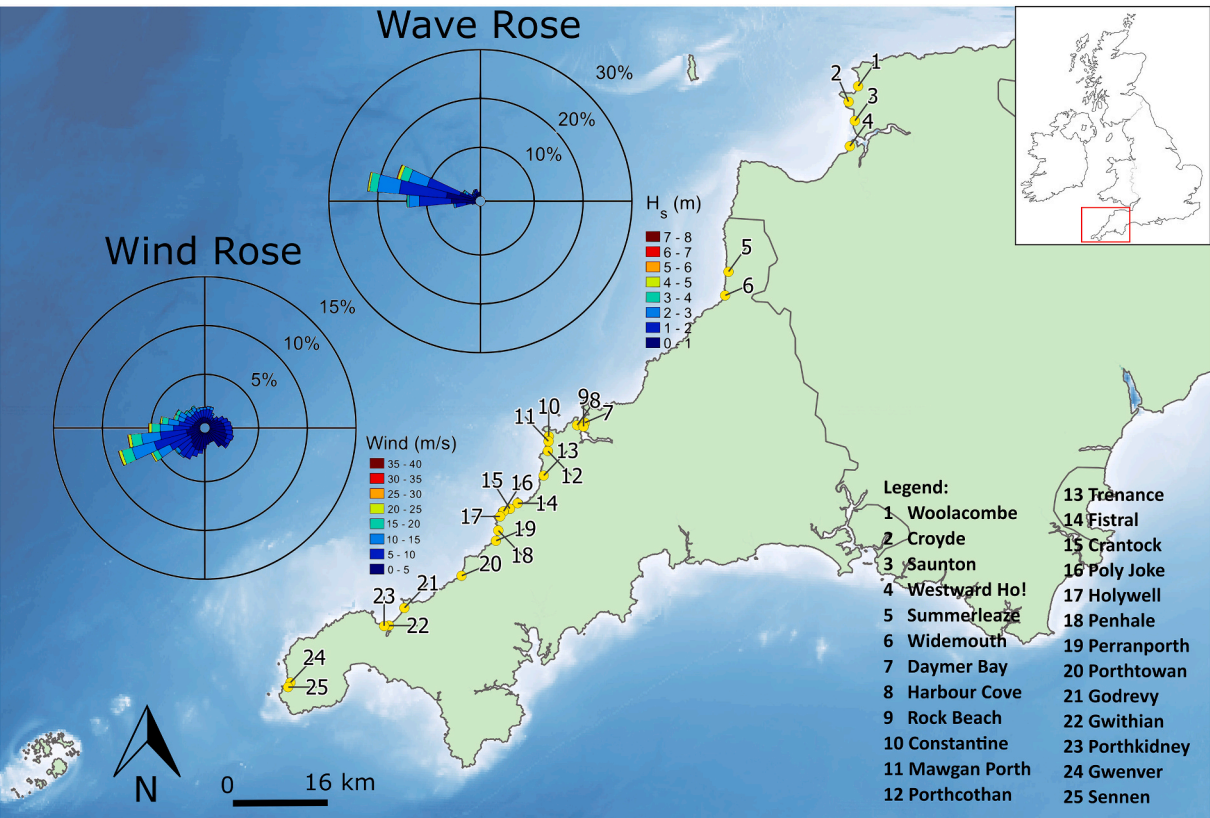
Fig. 1. Regional map of southwest England with the 25 dune sites shown. Wave (top) and wind (bottom) rose plots are included. These are generated from data (www.channelcoast.org) close to Perranporth (#19), located mid-way along the north coast and considered representative of the region. (For interpretation of the references to colour in this figure legend, the reader is referred to the web version of this article.)

Fig. 2. Aerial photographs of 18 of the 25 dune sites demonstrating wide variety in scale and setting. Thick white line in the lower part of the photographs represents 1-km scale bar.

Table 1

Summary table of each dune location and site characteristics including the data availability and relative exposure of each dune system. Shaded cells indicate sites where LiDAR and topographic profile data are available.

Dune Location	Dune Code	Alongshore length of embayment (km)	Data available for analysis		Relative Dune Exposure	
			Topographic profiles (6 monthly)	LiDAR	Orientation of shoreline (degrees)	Embaymentisation; ratio of alongshore length and depth of embayment
Woolacombe	Wool	2.10	No	Yes	280	2.0
Croyde	Croy	0.47	No	Yes	270	2.3
Saunton	Saun	3.90	No	Yes	270	6.2
Westward Ho!	Who!	0.50	No	Yes	260	6.2
Summerleaze	Summ	0.15	Yes	Yes	290	0.8
Widemouth	Wide	0.23	Yes	Yes	280	5.5
Daymer Bay	Daym	0.15	No	Yes	280	1.0
Rock	Rock	0.50	No	Yes	270	0.8
Harbour	Harb	0.47	No	Yes	360	0.5
Constantine	ConS/ConN	0.55	Yes	Yes	240/280	3.8
Treyarnon	Trey	0.09	Yes	Yes	310	1.9
Porthcothan	Porc	0.16	Yes	Yes	300	0.6
Trenance	Tren	0.25	Yes	Yes	290	1.2
Fistral	Fist	0.40	Yes	Yes	290	3.9
Crantock	Cran	0.60	Yes	Yes	310	0.4
Penhale	Penh	1.42	Yes	Yes	290	5.0
Perranporth	Perr	0.41	Yes	Yes	290	4.2
Poly Joke	Poly	0.06	No	Yes	350	0.6
Holywell	Holy	0.48	No	Yes	300	1.2
Porthtowan	PorT	0.07	Yes	Yes	310	2.7
Godrevy	Godr	0.19	Yes	Yes	280	2.5
Gwithian	Gwit	2.12	Yes	Yes	310	2.0
Porthkidney	PorK	0.82	Yes	Yes	350	1.5
Gwenver	Gwen	0.17	Yes	Yes	300	3.0
Sennen	Senn	0.47	Yes	Yes	300	2.7

Fig. 3. Two most contrasting dune settings along the north coast of SW England: (a) eroding dune system of Crantock with steep unvegetated front under energetic high tide conditions; and (b) prograding foredune systems of Harbour Cove at low tide.

Furthermore, historic sand mining in St Ives Bay has had a detrimental impact on the historically large Godrevy system; however, enhanced protection and dune management now facilitates recovery.

Each site was characterised in terms of their exposure, defined by shoreline orientation as the direction of the seaward tangent perpendicular to the shoreline alignment, and the degree of embaymentisation, defined by the ratio between the distance between flanking headlands L_{emb} and depth of the embayment D_{emb} determined using the high-tide shoreline (Table 1). This parameterisation is the reciprocal of the aspect ratio and planform ratio used by George et al. (2015) and Fellowes et al. (2019), respectively. A large embaymentisation value indicates a relatively open and exposed coast (e.g., Saunton), whereas a small value indicates a deep embayment and sheltered setting (e.g., Poly Joke). Note also that given a dominant Atlantic swell wave direction of 280° (Fig. 1), the closer the seaward tangent perpendicular to the

shoreline orientation is to that value, the more exposed the site is to energetic waves. Most dune sites are fully exposed (orientation 270°–290°), but some are oriented perpendicular to the prevailing wave direction (e.g., Porthkidney). All sites are plotted in an embaymentisation-orientation parameter space in Fig. 4 and a qualitative assessment has been made with respect to their degree of wave exposure based on their positioning in this parameter space and local knowledge.

3. Methods

3.1. PCO topographic profiles

The Southwest Regional Coastal Monitoring Programme has been providing comprehensive monitoring of the coastal environment in SW
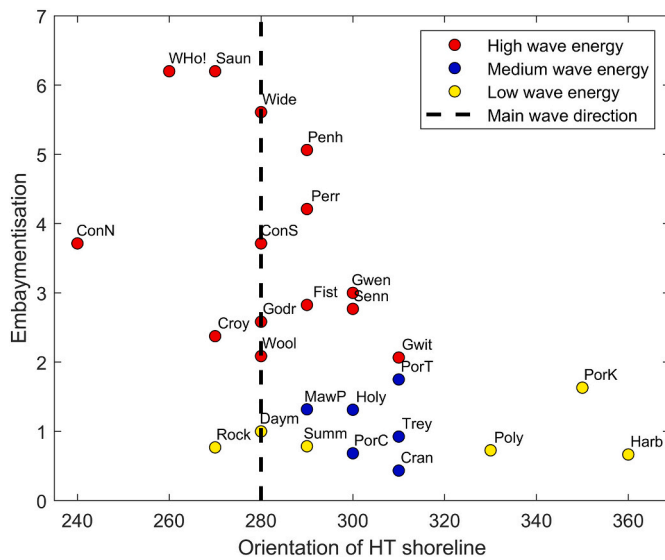
Fig. 4. Orientation and the degree of embaymentisation of the high tide shoreline for all dune sites. For site abbreviations, refer to Table 1. Wave energy classification is relative and based on site knowledge of local inshore wave conditions. Embaymentisation has been quantified as the ratio between the width of the embayment (distance between headlands) and the depth of the embayment (distance from line connecting headlands and high tide shoreline).

England since 2006, including topographic beach profile surveys and LiDAR, and data are freely available from the Plymouth Coastal Observatory (PCO) website (https://coastalmonitoring.org/southwest/). All dune sites along the north coast of SW England for which regular (6-monthly) topographic beach surveys are available have been investigated in terms of their intra-annual morphological variability. Multiple profile transects are generally available for each beach, but a single profile, considered most representative for the dune system, was selected at each site for analysis.

Different parameters can be extracted to characterise dune dynamics, and a key aspect is to separate the beach from the dune region, referred to here as the 'dune foot' (or 'dune toe'), which is widely used to map inter-annual to decadal dune dynamics (Ruessink and Jeuken, 2002; van Ijzendoorn et al., 2021). Identifying the elevation of the dune foot, is, however, far from trivial (Diamantidou et al., 2020; Smith et al., 2020). Here, an elevation of the dune foot of $z_{df} = 5$ m was selected, which broadly corresponds to the mean high water spring level plus 1–2 m, representing storm surge + maximum runup on these mainly dissipative beaches. Fig. 5 illustrates the appropriateness of such approach. The figure shows the first, last and all intermediate beach-dune profiles for one of the sites (Penhale) (Fig. 5a) and also the change in the position

of the various beach-dune elevation contours relative to that at the start of the surveys (Fig. 5b). The elevation contours associated with the supra- and intertidal beach region exhibit a very large variability over the decadal time scale in response to inter-annual changes in the wave forcing, largely described by the variability in the North Atlantic Oscillation (Masselink et al., 2014; Castelle et al., 2018), whereas the dune contour lines show consistent trends with limited variability. For Penhale, beach contour line variability is 40–60 m, whereas the dune contour lines are constrained within a 10-m band of variability, displaying a retreat of up to 15 m over the survey period (up to 1 m yr^{-1}).

For each dune site, the elevation separating the highly dynamic upper beach from the trend-sensitive dune region was defined as $z_{df} = 5$ m. A regional-scale dune foot elevation was selected as representative for all dune locations as accurate information on tide, surge and inshore wave conditions are not universally available. The sensitivity of the results to the selection of z_{df} will be addressed in Section 4.3. Dune volume Q was quantified by integrating the topographic profile above the elevation of the dune foot up to a fixed landward location common to all profiles for that dune site, and the time series of Q relative to that at the start of the survey was used to quantify the dune dynamics. Dune recession (or progradation) was quantified by determining the change in the cross-shore location associated with the z_{df} contour between the first and last surveyed profile for each site. It is noted that at several sites (e. g., Crantock), high dune scarps (> 10 m), were present which had significantly retreated over the survey period without clear evidence of retreat of the dune foot, representing a flattening of the dune face; nevertheless, dune change was consistently quantified with respect to the 5-m ODN contour line position.

3.2. Plymouth coastal observatory (PCO) LiDAR data

For all dune sites along the north coast of SW England for which LiDAR data are available, the filtered data at 1-m grid resolution were used to investigate dune dynamics. LiDAR offers superior spatial coverage compared to the topographic data, but are only collected every several years and here only the earliest (2007/08) and the latest (2017/18/19/20) datasets were used, representing epochs of 9–13 years. At each dune site, a rectangular Region of Interest (ROI) was identified, extending cross-shore from the top of the intertidal beach to what was considered the landward limit of dune activity, and longshore covering the greatest extent of the beach/dune system without including the headlands.

The LiDAR data were used to extract the same parameters as from the topographic data: dune volume Q and position of the dune foot x_{df} for the different LiDAR datasets, and then dQ and dx_{df}, representing the changes that have occurred over the epoch. The LiDAR data cover practically the entire width of the dune systems; therefore, dQ and dx_{df} were along-coast averaged to be more representative than the single values derived from the topographic profiles. LiDAR data has an
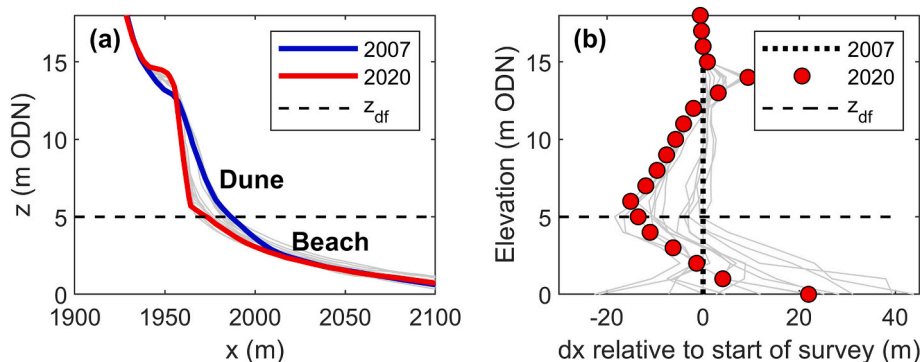

Fig. 5. (a) Beach profile change for a representative profile at Penhale from 2007 to 2020; and (b) variability in the cross-shore location dx of the contour lines from −2 m to 10 m ODN, relative to that at the start of the survey period. The elevation of the dune foot is defined as z$_{df}$.

inherent vertical inaccuracy δz_{DEM} of 0.15 m. This inaccuracy was taking into account when computing the uncertainties associated with the sediment volumetric change using the same methodology as deployed by Wiggins et al. (2019), including the removal of grid cells that displayed vertical change less than the limit of detection ($\sqrt{(\delta z_{DEM1} + \delta z_{DEM2})^2} = 0.21$ m). The inaccuracy associated with the dune foot location was considered δx_{df} of 1 m (LiDAR grid size), and propagating this uncertainty to a change in dune foot location yields ($\sqrt{(\delta x_{df1} + \delta x_{df2})^2} = 1.41$ m).

3.3. Exposure of the dune foot to wave conditions

For dune retreat to occur as a result of wave action, wave runup must reach the dune foot z_{df}. The total runup elevation zR (in m ODN) is the sum of four main components (Sallenger, 2000):

$$zR = R_{2\%} + \text{tide} + \text{residuals} + \text{SLR}$$

where $R_{2\%}$ = 2% exceedance runup height, tide = tidal elevation, residuals = non-tidal residuals (e.g., storm surge) and SLR = sea-level rise. Using a combination of sources, a 40-year time series of zR, representing the period 1980–2020 was derived. Met Office AMM7 wave data from the WWIII model for the node nearest to the Perranporth wave buoy, which is considered representative for most of the exposed north coast of SW England, was used to compute $R_{2\%}$ using the Stockdon et al. (2006) runup equation for dissipative beaches:

$$R_{2\%} = 0.0043(H_s L_0)^{0.5}$$

where $R_{2\%}$ represents the 2% exceedence runup height, H_s is the offshore significant wave height and L_0 is the deep-water wave length based on the peak wave period. No long-term tide measurements are available for Perranporth, so site-specific modelled data based on a short-term, locally measured field data set were used. The tidal signal was based on harmonic analysis of measured tide data at Perranporth from 2008 to 2010, but the non-tidal residuals were obtained from tidal data collected at Newlyn, located 40 km southwest of Perranporth. The Newlyn tide data were also used to derive a mean rate of sea-level rise by conducting a simple linear regression on the annually-averaged water level from 1980 to 2020. The resulting rate of sea-level rise is 0.0028 m yr^{-1}.

Three different 40-year time series of zR were constructed:

$$zR_1 = R_{2\%} + \text{tide}$$

$$zR_2 = R_{2\%} + \text{tide} + \text{residuals}$$

$$zR_3 = R_{2\%} + \text{tide} + \text{residuals} + \text{SLR}$$

The rationale behind using these different formulations for zR is to investigate the added importance of the non-tidal residuals and SLR, in addition to tide and wave forcing, in enhancing the potential for dune scarping.

Hourly time series of zR were constructed and these were then used to compute the dune scarping potential DSP by determining for each time step whether the runup exceeded the dune foot (taken as $z_{df} = 5$ m ODN) and, if so, the amount of 'excess runup energy', parameterised by $(zR-z_{df})^2$, which reached the dune foot. By plotting the cumulative time series of $(zR-z_{df})^2$ and the hours that the runup exceeds z_{df} for the different formulations of zR, the relative importance of the different contributing factors to the dune scarping potential (referred to as DSP_{energy} and DSP_{time}, respectively) can be assessed. This approach has only been applied to Perranporth because this is the only site with a wave buoy directly offshore and this site also has the best dune dynamics time series. The DSP approach has previously been applied in a different form to quantify exposure of coastal cliffs to wave action (Early et al., 2018) and is potentially transferable to other dune locations.

3.4. Application of Bruun rule to predict beach/dune retreat

Of all coastal settings, sandy beach/dune systems are probably the least unsuitable for application of a Bruun-rule approach to forecast coastal retreat as a result of sea-level rise (Bruun, 1954; Dean and Houston, 2016). The standard Bruun Rule is:

$$R = S\frac{W_*}{h_* + B} \tag{1}$$

where R is the amount of shoreline retreat over a given period, S is the amount of sea-level rise over that period, W_* is the width of the active shoreface, h_* is the morphological depth of closure and B is the berm height. The latter includes the height of any dunes present (Rosati et al., 2013). When expressed as a rate of retreat, Eq. (1) becomes:

$$\frac{dR}{dt} = \frac{dS}{dt}\frac{W_*}{h_* + B} \tag{2}$$

It was observed at many of the dune sites, that the dune face is retreating and that sediment is transported from the front of the dune to the top and back of the dune. We will refer to this process as 'dune roll-over', analogous to 'barrier roll-over', characteristic of gravel barrier response to sea-level rise (Orford and Carter, 1995).

Rosati et al. (2013) have modified the standard Bruun rule to account for this onshore sediment transport component by adding an extra term (see their Fig. 11 for definition sketch):

$$R = S\frac{W_* + V_D/S}{h_* + B} \tag{3}$$

where V_D is the amount of landward deposition (units per unit meter beach/dune length). Note that this extra term means that the amount of shoreline retreat increases due to this additional onshore transport component. In other words, dune roll-over enhances shoreline retreat. When expressed as a rate of retreat, Eq. (3) becomes:

$$\frac{dR}{dt} = \frac{dS}{dt}\frac{W_* + dV_D/dS}{h_* + B} \tag{4}$$

where dV_D represents an volumetric onshore sediment transport amount over the a time interval dt and dS represents a sea-level increment over that same time interval.

A recent approach suggested by Davidson-Arnott and Bauer (2021) considers dune retreat to be simply proportional to the ratio between the amount of sea-level rise S and the slope of the beach $\tan \beta$ after a major storm.

$$R = \frac{S}{\tan\beta} \tag{5}$$

We intend to use Eqs. (1), (3) and (5) to compare projected shoreline retreat rates with observations. Rather than dealing with (to some degree unquantifiable) site-specific factors and circumstances, and conducting separate computations for each dune location, regionally-averaged parameter values with an estimated variability around the mean will be used. We assume that the parameters have a triangular probability distribution described by the minimum, median and maximum parameter values. We will use a Monte Carlo approach to compute 10,000 separate realisations of the parameter set to derive a distribution of shoreline retreat from which statistical properties can be computed (Cowell et al., 2006; Vitousek et al., 2017; Vousdoukas et al., 2020; Mccarroll et al., 2021). Table 2 lists the parameter values and their source.

4. Results

4.1. Topographic data

Fig. 6 shows results of topographic analysis of all sites with regular

Table 2

Minimum, mean and maximum values for the environmental parameters used in the application of the Eqs. (1), (3) and (5) for predicting shoreline retreat as a result of sea-level rise, and the source of this information.

Parameter	Units	Description	Min	Median	Max	Source
dS/dt	m yr^{-1}	Rate of current sea-level rise	0.002	0.003	0.004	Newlyn tide gauge
$W*$	m	Width of active shoreface	500	1000	2000	Valiente et al. (2019)
$h*$	m	Depth of active shoreface	5	10	15	Valiente et al. (2019)
B	M	Berm height (incl. dune)	3	8	15	This study
V_D/dt	m^2 yr^{-1}	Onshore volumetric sediment transport rate	0	2	4	This study
$\tan \beta$		Beach gradient after major storm	0.01	0.015	0.025	Field observations made over past decades by authors
dS	m	Future amount sea-level rise (by 2100)	0.44	0.60	0.76	IPCC (2021) forecast for SSP2–4.5

survey data. The variety in dune morphology (Fig. 2) and settings (Fig. 4) is reflected in the wide range of dune morphological responses recorded over the last 10–15 years along the north coast of SW England. In terms of dune volumetric change, of the 16 dune sites with topographic transects, four experienced considerable accretion ($dQ > +10$ m^3 m^{-1}; e.g., Summerleaze), three showed very limited change ($|dQ| < 10$ m^3 m^{-1}, e.g., Treyarnon) and nine experienced considerable sediment losses ($dQ < -10$ m^3 m^{-1}; e.g., Fistral). For the dune sites with losses in dune volume of >10 m^3 m^{-1}, most of the loss generally occurred during the 2013/14 winter (e.g., Penhale), which was the most energetic winter since at least 1948 (Masselink et al., 2016b). However, for some locations other winters are also important, e.g., the 2009/10 winter for Porthkidney and the 2016/17 and 2017/18 winters for Crantock.

The change in the dune foot position over the monitoring period also varied widely with four sites experiencing considerable advance ($dx_{df} > +5$ m; e.g., Gwenver), four sites showing very limited change ($|dx_{df}| < 5$ m; e.g., Sennen) and eight sites experiencing considerable retreat ($dx_{df} < -5$ m; e.g., Crantock). Notably, losses in dune sediment volume are not necessarily associated with dune retreat or vice versa (e.g., Perranporth), although the signs for dx_{df} and dQ can be the same (e.g., Porthcothan, Constantine South).

The 6-monthly topographic profiles are useful in providing an overview of the different dune dynamics, especially the timing of major forcing events. However, dune dynamics are often highly spatially variable and the representativeness of single profiles, such as presented in Fig. 6, can be questioned. Therefore, along-coast averaged dune parameters, such as derived from the LiDAR data presented in the next section, are considered more representative.

4.2. LiDAR data

Fig. 7 shows examples of difference DEMS based on LiDAR data for eight of the 26 dune sites with such data available. Again, the wide variety in dune response patterns is apparent, ranging from relatively along-coast uniform dune retreat (e.g., Fistral, Porthkidney) or dune progradation (e.g., Harbour, Constantine), to a very significant along-coast variable response due to the presence of dune blow-outs (e.g.,

Crantock, Holywell, Perranporth). The difference DEM for Woolacombe shows a dune response characterised by simple dune retreat at its southern end, but sediment deposition landward of a retreating dune face at its northern end. As illustrated in the next section, such dune roll-over response is commonly observed and explains to some degree why significant dune retreat is not automatically associated with significant losses in dune sediment volume.

The key dune change parameters dx_{df}/dt and dQ/dt derived for each of the dune sites with LiDAR data have been compared within their environmental context in Fig. 8. There are almost as many sites with dunes that have increased in volume (12 out of 25) than those that have decreased in volume (13 out of 25). On the other hand, for 19 of the 25 sites the dune foot has retreated, and the two sites with the largest rate of dune progradation (Harbour, Poly Joke) are amongst the most sheltered environments. Therefore, the vast majority (16 out of 20) of the dune sites exposed to medium or high wave energy (cf., Fig. 4) have experienced dune retreat. The average amount of dune retreat dx_{df} for all dune sites experiencing dune retreat is 5.5 m ($+/- 4.1$ m), which converts to a rate dx_{df}/dt of 0.4–0.6 m yr^{-1} considering a 9–13 year monitoring period. Many of these sites are characterised by a positive dune sediment budget, suggesting that in many cases the mechanism of dune retreat is roll-over, characterised by sediment removal from the frontal dune and deposition on the back of the dune, and henceforth referred to as 'dune roll-over'.

4.3. Dune foot exposure

Fig. 9 evaluates the dune scarping potential *DSP* over the period 1980–2020 based on the wave and water level conditions for Perranporth and considering events during which the runup elevation exceeds the elevation of the dune foot $z_{df} = 5$ m ODN. Wave runup reaches the dune foot practically every year and, as expected, the winter of 2013/14 stands out as a particularly energetic winter with the predicted runup elevation exceeding the dune foot by almost 1.5 m during one storm event (Fig. 9a). There seems to be a trend of increased runup elevations over time, which is a result of a 0.12-m rise in sea level over the 40-year period, compounded by increased storminess (Castelle et al., 2018).

When only considering the contributions of wave runup and tide to the runup elevation, the regionally-representative dune foot is subjected to wave action for 138 h over the 40-year modelled period (zR_1 in Fig. 9b). Adding the contributions of the non-tidal residuals (zR_2) and sea-level rise (zR_3) to the total runup, increases the exposure of the dune foot to wave action to 226 and 296 h, respectively. A similar increase in dune scarping potential when residuals and sea-level rise are added is apparent when the amount of runup energy at the dune foot is considered (Fig. 9c). The total amount of 'excess runup energy' experienced at the dune foot for zR_1, zR_2 and zR_3 is 13.9, 24.4 and 34.3 m^2, respectively. The conclusion of this analysis is that both the non-tidal residuals (i.e., storm surge) and the sea-level rise (SLR) significantly enhance the potential for dune scarping, regardless of whether duration of runup action (ΣDSP_{time}) or energy of runup action (ΣDSP_{energy}) is considered. In the context of this paper, the increase in *DSP* when considering sea-level rise is of most relevance, and the percentage increase in ΣDSP_{time} and ΣDSP_{energy} when comparing zR_2 (without SLR) and zR_3 (with SLR) is 31% and 41%, respectively.

Simulations were also carried out with a dune foot elevation 0.5 m lower and higher. For $z_{df} = 4.5$ m and $z_{df} = 5.5$ m, the values for ΣDSP_{time} and ΣDSP_{energy} are almost an order of magnitude larger and smaller, respectively, than for $z_{df} = 5$ m. For example, for the zR_3 scenario, ΣDSP_{time} for $z_{df} = 4.5$, 5 and 5.5 m is 1837, 296 and 44 h, respectively (reflecting 45, 7 and 1 h per year). The very large (small) number of hours of runup action at the dune foot for the lower (higher) z_{df} threshold suggests that $z_{df} = 5$ m is an appropriate dynamic threshold separating the wave-dominated beach from the wind-dominated dune as it provides an appropriate balance between magnitude and frequency of runup action.
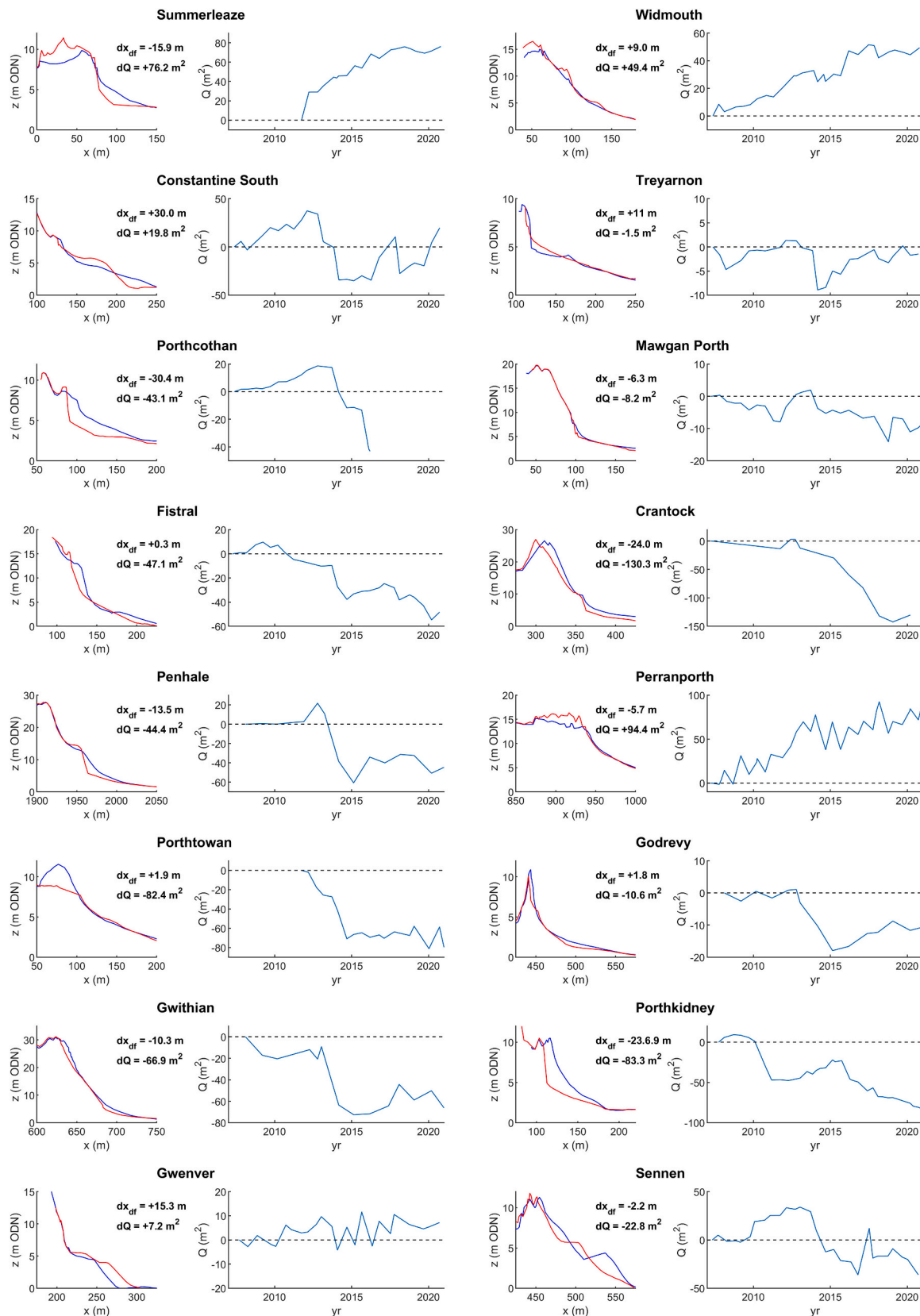
Fig. 6. Analysis of PCO topographic survey data for all dune sites with regular (i.e., six-monthly) survey data. Blue and red lines in the left panels represent the first (usually 2006 or 2007) and last (usually 2019 or 2020) available topographic survey, respectively. The right panels for each of the dune sites plots the time series of the sediment volume Q above the dune foot ($z_{df} = 5$ m ODN) relative to that at the start of the survey. The amount of change in the dune foot position and dune volume between the last and first survey is represented by dx_{df} and dQ, respectively, with a negative value representing dune retreat and dune volume loss. (For interpretation of the references to colour in this figure legend, the reader is referred to the web version of this article.)
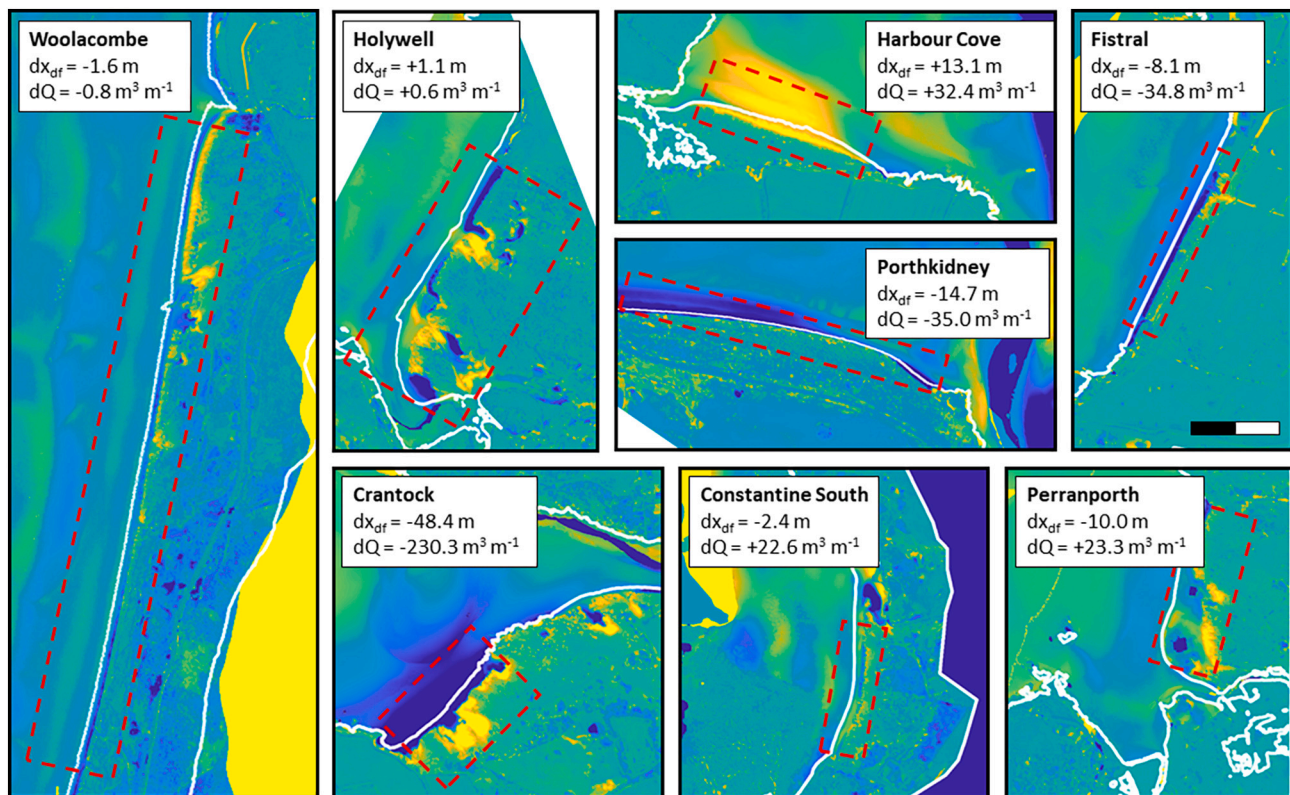
Fig. 7. Selection of difference DEMs based on LiDAR data, representing c. 10-year epochs. Colour map runs from −2.5 m (dark blue) to +2.5 m (bright yellow), with green representing no change; the white line represents the 5 m ODN elevation contour at the start of the epoch, representing the dune foot; and the red rectangle indicates the region of interest over which the dune change has been computed, with dx_{df} representing the alongshore-averaged change in dune foot position and dQ representing the change in dune sediment volume. All DEMs have the same scale and the scale bar in the upper-right panel represents 200 m. The two dark patches in the Perranporth plot represent buildings that were only filtered in the earliest LiDAR data set; these regions have not been considered in the computation of dune volume change. (For interpretation of the references to colour in this figure legend, the reader is referred to the web version of this article.)

4.4. Analysis of biennial LiDAR data for Penhale

The 6-monthly topographic data presented in Section 4.1 provides good temporal resolution, but only for single cross-shore profiles. Three-dimensional dune dynamics are captured by the LiDAR data discussed in Section 4.2, but generally lack temporal resolution. This makes it challenging to validate the modelling approach described in Section 4.3 and to demonstrate that more energetic periods are associated with dune retreat, and less energetic periods with recovery. In order to address this issue more comprehensively, LiDAR data at high temporal resolution are needed which include both stormy and quiescent meteorological phases, and not simply LiDAR data from the start and end of a decadal monitoring period.

Of the study sites reported here, Penhale has the best LiDAR coverage (2008, 2012, 2014, 2016, 2017, 2018 and 2020), allowing a greater degree of temporal constraint on shoreline change analysis than possible at other sites. Penhale is also in the large group of dunes experiencing chronic overall volume loss and is considered representative of most exposed and eroding dune sites along the north coast of SW England. Comparison between the 2008 and 2020 LiDAR digital elevation model, representing a 12-year period, shows a near-continuous retreat of the frontal dune (linear red/yellow feature in Fig. 10a). In addition, the evolution of the large blow-out at the southern end of the dune area is also clearly visible (red/blue feature in Fig. 10a).

Using the datum-based 5-m ODN contour shoreline proxy extracted from LiDAR, Fig. 10c shows the location of the shoreline along a 400-m stretch of coast, representing the northern section of Penhale, for all available LiDAR data. Average shoreline retreat computed over a 1-km section of dune, including the shorter 400-m section shown in

Fig. 10c, over the 2008–2020 period was 10.9 m (0.9 m yr^{-1}), but this record contained periods of quasi-stasis in shoreline position between 2008 and 2012 (1.6 m advance; 0.4 m yr^{-1}) and large shoreline retreat from 2012 to 2014 (15.1 m retreat; 6.3 m yr^{-1}). Fig. 10c also shows that between 2014 and 2017 there appears to have been a progressive seaward advance in the 5-m contour, by an average of 7.46 m (2.9 m yr^{-1}). Field observations suggests this is due to the creation of a small berm building against the dune face. DEMs of difference show alongshore dune accretion between 2014 and 2017 of over 1 m for extensive stretches landward of the 5-m contour (Fig. 10b). As the shoreline advances, the beach-dune sediment transport pathway re-connects and sediment is returned to the dune. The 5-m contour retreated landward in the period 2017 to 2020, by 5.0 m (1.4 m yr^{-1}).

The relatively high-resolution LiDAR data for Penhale (cf. Fig. 10) offers the opportunity to link wave/runup processes (cf. Fig. 9 to dune dynamics. Using the modelled runup time series zR (Fig. 11a), the dune scarping potential, parameterised by ΣDSP_{time} and ΣDSP_{energy} (cf. Section 4.3) was integrated over each of the LiDAR epochs (2008–2012, 2012–2014; 2014–2016, 2016–2017, 2017–2018, 2018–2020) and converted into an annual amount (ΣDSP_{time} in number of hrs per year; ΣDSP_{energy} in m^2 per year). These annual amounts of dune scarping potential were then correlated with the observed amount of dune foot retreat dx_{df} (Fig. 11b), converted to a retreat rate dx_{df}/dt (in m per year). The results indicate that the amount of runup energy reaching the dune foot is related to the amount of recorded dune foot retreat. The dune system at Penhale shows significant retreat when wave runup reaches the dune foot for >15 h per year ($\Sigma DSP_{time} >$ 15 h (Fig. 11c) and when the amount of 'excess runup energy' ΣDSP_{energy} exceeds 25 m^2 per year (Fig. 11d). The correlations between the *DSP* parameters and dune
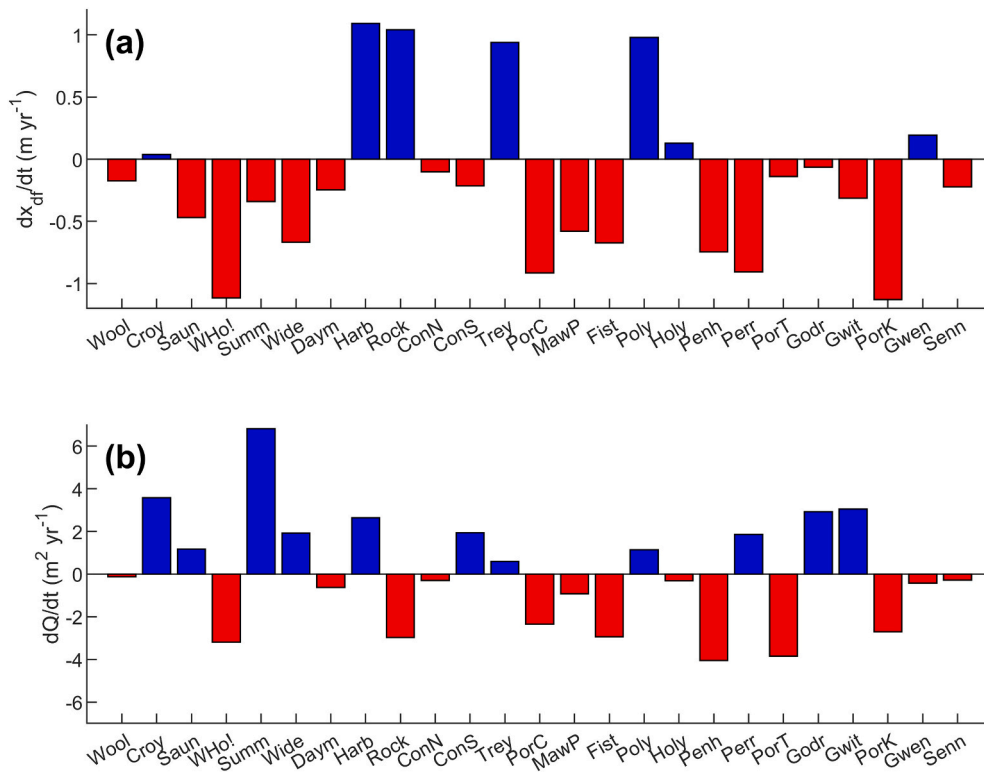
Fig. 8. (a) Rate of dune foot change dx_{df}/dt and (b) rate of dune volumetric change volumetric change dQ/dt for all dunes sites over 9–13-year period based on LiDAR data. (c) Scatter plot of dx/dt versus dQ/dt with uncertainty values indicated by the horizontal and vertical lines. Crantock is not included in this figure due to the extreme rate of dune foot retreat ($dx_{df}/dt = -4.8$ m yr^{-1}) and dune volume loss ($dQ/dt = -23.2$ m^3 m^{-1} yr^{-1}), and the site-specific reason for this (Hird et al., 2021).
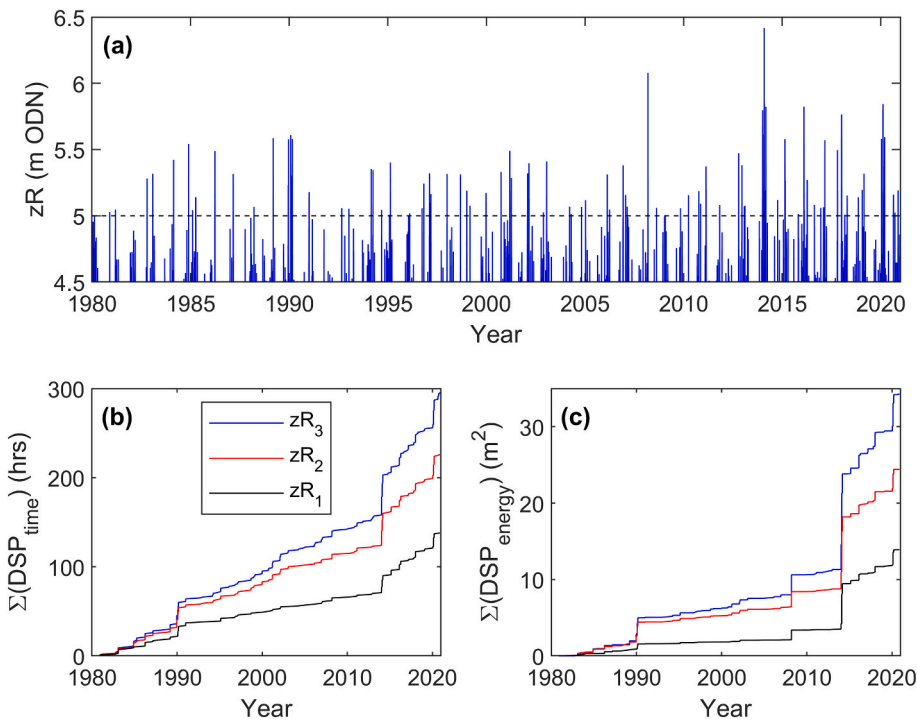

Fig. 9. Exploration of dune scarping potential for the period 1980–2020. Upper panel shows time series of total runup elevation zR (runup height + tide + residuals + sea-level rise) with the dashed line indicating the elevation of the dune foot $z_{df} = 5$ m ODN. The lower-left panel shows the time series of the cumulative number of hours with $zR > z_{df}$ showing the dune scarping potential in terms of time ΣDSP_{time}. The lower-right panel shows the time series of the cumulative runup energy associated with $zR > z_{df}$ showing the dune scarping potential in terms of energy ΣDSP_{energy}. The three lines in the lower panel represent: $zR_1 = R_{2\%} + $ tide; $zR_2 = R_{2\%} + $ tide + residuals; and $zR_3 = R_{2\%} + $ tide + residuals + sea-level rise.

retreat are significant ($p = 0.09$ for ΣDSP_{time}; $p = 0.02$ for ΣDSP_{energy}), but the number of data points considered is small ($N = 6$). Moreover, the trend lines fitted to the data are highly site-specific and aeolian processes are not included in this analysis. Nevertheless, this analysis clearly shows that the amount of runup energy that reaches the dune foot on an annual basis is a key factor in controlling frontal dune dynamics at the site.
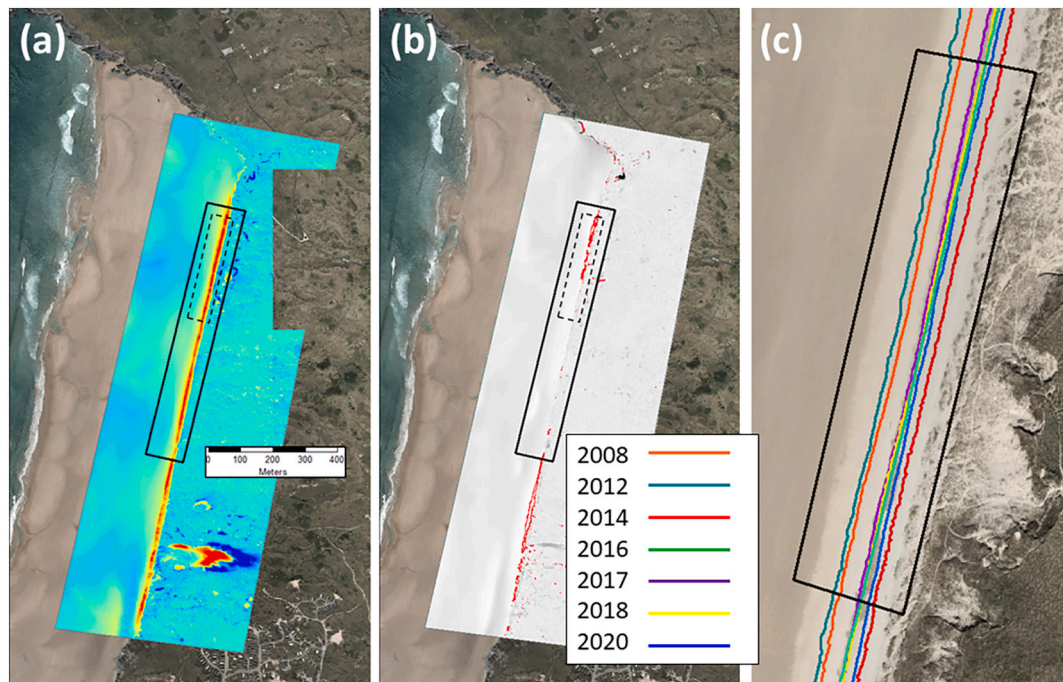
Fig. 10. LiDAR analysis of the dune system at Penhale over the period 2008–2020. (a) Morphological change over the 12-year period with red and blue denoting erosion and accretion, respectively. The large rectangle represents a 1-km section of dune for which dune retreat parameters have been computed; the small rectangle is the region plotted in (c) and represents a 400-m section. (b) Locations where dune top accumulation exceeded 1 m over the post-storm recovery period 2014–2017. (c) Position of the 5-m ODN contour (base of the dune foot) for a short section of dune. (For interpretation of the references to colour in this figure legend, the reader is referred to the web version of this article.)
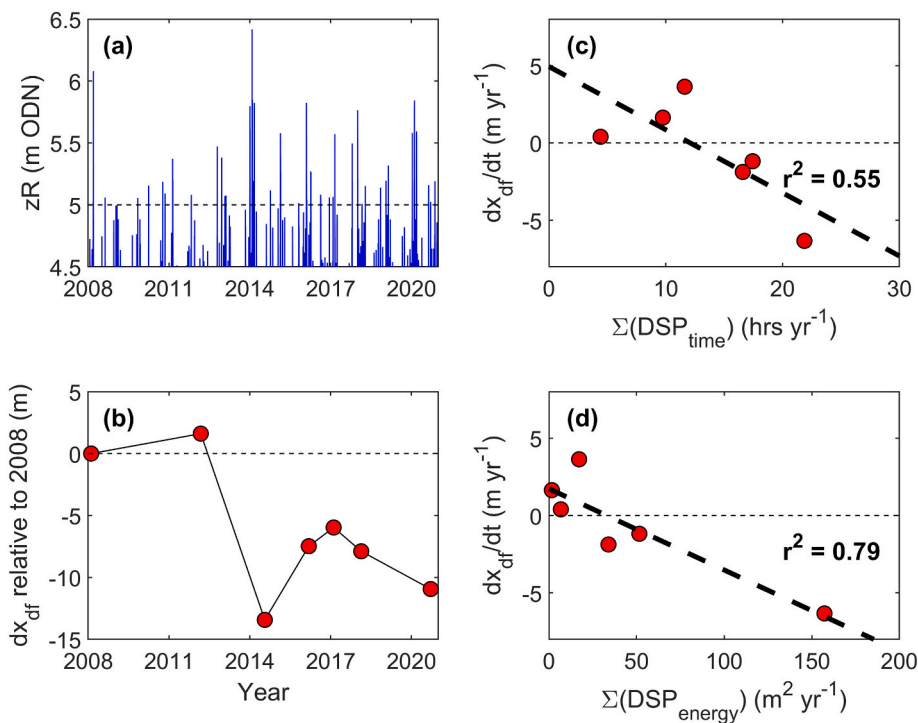

Fig. 11. Relation between dune scarping potential and observed dune retreat at Penhale for the period 2008–2020. (a) Time series of total runup elevation zR (runup height + tide + residuals + sea-level rise) with the dashed line indicating the elevation of the dune foot $z_{df} = 5$ m ODN. (b) Time series of the dune foot position dx_{df} relative to that at 2008 based on LiDAR data (cf. Fig. 10). Scatter plot with line of best fit between: (c) number of hours with $zR > z_{df}$ per year and annual retreat rate of dune foot dx_{df}/dt; and (d) runup energy associated with $zR > z_{df}$ per year and annual retreat rate of dune foot dx_{df}/dt.

4.5. Hindcasting dune retreat

The globally-used (Vousdoukas et al., 2020), albeit contentious (Cooper et al., 2020), Bruun rule was applied to explore the amount of historic dune retreat as a result of sea-level rise using the probabilistic approach outlined in Section 3.4. Considering regionally-averaged

environmental parameters and accounting for inter-regional variability, and applying the standard Bruun rule (Eq. (2)), results in a median dune retreat rate of 0.12 m yr^{-1}, with a 5–95% uncertainty band of 0.06–0.23 m yr^{-1}. Accounting for the onshore sediment transport into the dunes due to dune roll over (estimated at 2 m^3 m^{-1} yr^{-1}), and using the modified Bruun rule (Eq. (4)), doubles the median rate of dune

retreat to 0.23 m yr^{-1} (0.13–0.38 m yr^{-1}). The recent approach suggested by Davidson-Arnott and Bauer (2021) considers dune retreat simply proportional to the ratio between the amount of sea-level rise and the slope of the beach after a major storm. Applying this model probabilistically, results in a hindcasted dune retreat rate of 0.13 m yr^{-1} (0.08–0.20 m yr^{-1}). Over the 9–13-year period covered by the LiDAR data, these dune retreat rates represent amounts of retreat according to the Bruun rule of c. 1.3 m ignoring sediment transport into the dunes and c. 2.5 m when accounting for onshore transport, and c. 1.4 m according to the Davidson-Arnott and Bauer (2021) approach.

The actual dune retreat values over the observational period, taking into account all eroding dune systems, is c. 5.5 m, which is considerably higher than the hindcasted values obtained from the dune retreat models. Apart from shortcomings in the modelling approach, including assuming sediment continuity and disregarding potential sediment losses to the longshore and/or offshore, an additional factor may be the occurrence of a number of extreme storms over the last decade, especially the 2013/14 winter (cf. Fig. 9) which could have accelerated dune retreat.

5. Discussion

The dune systems along the north coast of the SW England show considerable variability in wave exposure, related to a combination of embaymentisation and shoreline orientation (Fig. 4) (Scott et al., 2011; King et al., 2021). The vast majority of dune systems appear relatively sediment-poor in that many of them typically exist as relatively thin sediment deposits overlying solid bedrock ('climbing dunes'; Fig. 12a). A variety of dune responses, expressed as changes in the position of the dune foot (at z = 5 m ODN) and in the dune volume above the dune foot, was observed. The direction of dune foot movement is not universally related to the dune sediment budget (Fig. 8b), and almost half of the retreating dune systems are characterised by a positive sediment budget. Dune foot progradation was found mainly for the sheltered dune systems (up to 1 m yr^{-1}), while the vast majority of exposed dune systems experienced dune foot retreat (up to 1.5 m yr^{-1}). Dune volumetric

changes, computed over whole dune systems and based on analysis of LiDAR data, ranged from −5 m^3 m^{-1} yr^{-1} to +8 m^3 m^{-1} yr^{-1}. In comparison, Costas et al. (2020) found rates of dune top accumulation from Ancão, Portugal, of 0.5–5 m^3 m^{-1} yr^{-1}, whereas de Vries et al. (2015) and Donker et al. (2018) observed sediment accumulation rates along the coast of The Netherlands of 10–40 m^3 m^{-1} yr^{-1}.

The retreating dune systems along the north coast of the SW England are not given to developing foredunes, but are generally fronted by rectilinear or concave sand ramps (Fig. 12b). These ramps experience undercutting, scarping and retreat whenever runup exceeds the elevation of the dune foot (Figs. 3a and 12c). Topographic profile data since 2006 suggest that many of the exposed dune systems are in a state of ongoing volumetric loss (Fig. 6) (e.g., Fistral, Penhale and Porthkidney). However, there is also evidence of non-linear responses, with some dunes experiencing alternating periods of either accumulation or loss, but resulting in net sediment gain over time (e.g., Summerleaze, Widemouth, Perranporth). A third group of sites (e.g., Constantine South, Treyarnon, Gwenver) appear stable and show neither net gain nor loss of sediment over time. While the topographic profiles give a well-constrained temporal signal, they lack the detailed spatial coverage that shows how the dune systems as a whole have responded to recent sea-level rise and storm impacts. Using LiDAR data (first and last available), several of the retreating dune systems, especially those characterised by volumetric gains, show dune roll-over (cf. Aagaard et al., 2004; Brooks et al., 2017), characterised by a combination of dune front scarping and retreat, and dune top accumulation (Fig. 7).

The exposed beaches in the study area are all characterised by wide expanses of sand at low tide (Fig. 2) and an energetic onshore wind climate (Fig. 1). The predominant occurrence of dune retreat is perhaps surprising. However, many studies have identified that full aeolian sediment transport potential is rarely achieved on beaches (Jackson and Cooper, 1999; Davidson-Arnott and Bauer, 2009; Costas et al., 2020; Sherman and Li, 2012), and that both sediment supply and connected transport pathways are important in facilitating dune recovery and/or foredune development. The intertidal region at all studied sites is often saturated (Fig. 12d), even during low tide. This inhibits aeolian

Fig. 12. Dunes of the north coast of SW England showing: (1) shallow aeolian deposits atop rocky outcrops; (b) dune ramp with few fixing objects; (c) alongshore dune scarping from 2013/14 extreme winter; and (d) variation in beach moisture of the upper supratidal beach (photos: 01/10/2016).

sediment transport (Ruz and Meur-Ferec, 2004; Hoonhout and de Vries, 2017; Brakenhoff et al., 2019), since higher moisture contents are associated with higher threshold wind velocity (> 9 m s^{-1}) for sediment entrainment (Belly, 1962). According to Costas et al. (2020), factors maximizing sediment transfer from the beach to the dune include a large backshore width, low runup excursion, and a gentle beachface and backshore gradient. On the other hand, sediment transport pathways are interrupted by poorly sorted sediment and/or surface armouring on the beach. Crucially, the presence of a beach scarp, a steep beach slope or a dune ramp (Fig. 12c), inhibits sediment transfer to the dunes, while a scarped dune entirely eliminates such potential transfers (Christiansen and Davidson-Arnott, 2004). Thus, despite the apparent abundance of sand on the beaches along the North coast of SW England, the amount of sediment available for aeolian transport could be limited due to the high moisture content of the sand and the sediment transport pathways are sub-optimal due to a lack of backshore and the presence of steep dune ramps and dune scarps.

The observed long-term (decades) dune retreat rate has been compared with hindcasted projections based on the Bruun rule. With the standard Bruun rule suggesting a regionally-averaged dune retreat of 0.06–0.23 m yr^{-1} and the modified Bruun rule (accounting for onshore sediment transport into the dunes) giving 0.13–0.38 m yr^{-1}, it appears that the observed regionally-averaged retreat rate (0.5 m yr^{-1}) exceeds these predictions by more than two-fold. Observed dune retreat rates were 2–3 times larger than predicted using simple parametric retreat models forced by sea-level rise. This suggests that the retreat models are inappropriate and/or that sea-level rise in itself may be insufficient to explain the observed retreat and that increased winter storminess may be implicated. The 2013/14 winter was the most energetic winter since 1948 (Masselink et al., 2016b) and the winter-wave climate across the Northeast Atlantic has increased in intensity and variability over the period 1949–2017 (Castelle et al., 2018).

The greater temporal and spatial resolution of the analysis presented for the representative dunes of Penhale (Fig. 10) has allowed us to further constrain long-term behaviour into periods of significant dune scarping during storms (2013–14 and 2017–2020) interspersed with periods of stasis (2008–12) and dune accretion (2014–17), but with a long-term tendency for shoreline retreat and upward accretion of the dune system. The analysis for the Penhale dune system further shows that the amount of runup energy that reaches the dune foot on an annual basis is a key factor in controlling frontal dune dynamics (Fig. 11). As sea-level rise accelerates in the near-future, it is expected that higher water levels will result in increased frequency of waves reaching the dune foot (Fig. 9), resulting in the resetting of the dune base to a more landward position. This seems to have occurred over the period 2008–2020.

Dune retreat will be amplified if wave conditions also become more stormy, resulting in increased runup levels, parameterised by R$_{2\%}$. A period of quiescence of 3–5 years, such as occurred during 2008–12 and 2014–17, can result in upper beach re-establishment and dune growth until scarping again occurs under extreme storms, such as occurred during the 2013/14 and 2018/20 winters. Important considerations are the timing in storm occurrence with respect to tidal levels and the clustering of storm events in time (Karunarathna et al., 2013). Dune scarping potential *DSP* in terms of excess wave energy reaching the dune foot (and integrated over time using hourly time series) for the 1980–2020 period has been quantified here as 13.9 m^2 (runup and tide), 24.4 m^2 (runup, tide and surge residual) and 34.3 m^2 (runup, tide, surge residual plus sea-level rise). It is clear that this energy increases steeply under extreme storms, as in 1990, 2008 and 2013–14. The additional 10.5 m^2 from surge effects and 9.9 m^2 from SLR over what would occur from tide and runup alone mean that the dune foot equilibrium line will be forced landward both as an acute and chronic response. The observed cyclicity in dune advance and retreat is forced by the winter storminess, which, in turn, is modulated by the North Atlantic Oscillation (Masselink et al., 2014; Castelle et al., 2017; Castelle et al., 2018). It is important to consider both shoreline advance and retreat, process mechanisms and sediment supply, when evaluating how dunes will respond to future changes in sea level rise and storms.

Based on Newlyn tide gauge data, regional sea-level has risen 3 ± 1 mm yr^{-1} since 1980, against a historical baseline rate of <2 mm yr^{-1} (WCRP, 2018), and intermittent, but significant stormy seasons frequently occur (e.g., 1990/1, 2008/9, 2013/14, 2019/20). Sea-level rise acceleration is projected to result in a rise in global mean sea level by 0.44–0.76 m according to the intermediate emission scenario SSP2–4.5 (IPCC, 2021). Therefore, the wave energy reaching the base of the dunes, instrumental in causing dune retreat (Fig. 11), will also increase, regardless of whether the observed increase in NE Atlantic storminess (Castelle et al., 2018) will persist over the remainder of this century (Fig. 9). This study thus provides a relatively conservative view of what future dune development in the study region might look like.

Simple extrapolation of the current regional trend in dune retreat of 0.5 m yr^{-1} will result in a regional dune retreat by 2100 of 40 m. Assuming a standard and modified Bruun rule approach, an amount of sea-level rise by 2100 of 0.44–0.76 m (median value of 0.6 m) according to the IPCC SSP2–4.5 scenario (IPCC, 2021) and the probabilistic approach outlined in Section 3.4 results in regional dune retreat by 2100 of 36.5 m (20.4–63.9 m) and 45.0 m (27.1–75.0 m), respectively. The recent approach proposed by Davidson-Arnott and Bauer (2021) predicts 39.9 m (30.2–54.3 m) of dune retreat by 2100. All these forecasts are based on simplistic models and assume sediment continuity and ignore alongshore spatial variability, the shallowness of the dune sediments and future changes in storminess. Despite this, these probabilistic approaches show a surprising level of agreement. Thus, in the absence of more robust and practical coastal retreat models that include dunes, they do serve to provide useful benchmarks for future coastal planning and management.

6. Conclusion

1. We investigated the decadal-scale, inter-annual dynamics of 25 coastal dune systems along the embayed, exposed and macrotidal north coast of SW England using a combination of topographic data and modelled wave conditions. The vast majority of the studied dune systems are fronted by rectilinear or concave sand ramps. These ramps experience undercutting, scarping and retreat whenever runup, usually during high-tide storm conditions, exceeds a critical dune foot elevation.

2. Practically all studied dune systems experience retreat with a regionally-averaged retreat rate of the dune foot of 0.5 m yr^{-1}. The majority of retreat occurred over a small number of especially energetic winters and it was found that dune retreat is not automatically linked to dune volumetric change. Many of the retreating dune systems display so called 'dune roll-over', characterised by removal of sediment from the dune face and deposition at the dune top.

3. A key factor in driving dune retreat along this coast is considered to be the number of hours that waves reach the dune foot or the excess runup energy present at the dune foot elevation. Along beach-dune systems, both sea-level rise and enhanced storminess will increase exposure of the dune foot to energetic wave action and this is expected to accelerate dune retreat rates in these settings.

4. Observed dune dynamics were compared with that hindcasted from simple parametric models forced by sea-level rise, including the Bruun Rule. Observed dune retreat rates were 2–3 times larger than predicted, suggesting that the retreat models are inappropriate and/or that sea-level rise in itself may be insufficient to explain the observed retreat and that increased winter storminess may be implicated.

5. For a sea-level rise of 0.6 m (0.44–0.76 m; SSP2–4.5) by 2100, the parametric shoreline retreat models predict c. 40 m of dune retreat with a very considerable range in retreat (20–75 m), resulting from uncertainty in model choice and parameterisation. The fact that at

many locations the dune sediment represents a relatively thin cover on top of a rocky substrate adds uncertainty to extrapolating historic dune recession rates. Simply extrapolating the current dune retreat rate also results in c. 40 m of dune retreat by 2100, but this approach ignores the potential acceleration in dune retreat rate due to an increase in the rate of sea-level rise.

6. The combination of analysis of multi-annual coastal dune morphological change and wave conditions, along with application of dune retreat models can provide useful insights into future dune evolution for coastal planners and managers.

Declaration of Competing Interest

The authors declare that they have no known competing financial interests or personal relationships that could have appeared to influence the work reported in this paper.

Acknowledgments

References

Aagaard, T., Davidson-Arnott, R., Greenwood, B., Nielsen, J., 2004. Sediment supply from shoreface to dunes: linking sediment transport measurements and long-term morphological evolution. Geomorphology 60, 205–224.

Backstrom, J., Jackson, D., Cooper, A., Loureiro, C., 2015. Contrasting geomorphological storm response from two adjacent shorefaces. Earth Surf. Process. Landf. 40, 2112–2120.

Belly, P.-Y., 1962. Sand Movement by Wind. California Univ Berkeley Inst of Engineering Research.

Brakenhoff, L.B., Smit, Y., Donker, J.J.A., Ruessink, G., 2019. Tide-induced variability in beach surface moisture: observations and modelling. Earth Surf. Process. Landf. 44, 317–330.

Brooks, S.M., Spencer, T., 2012. Shoreline retreat and sediment release in response to accelerating sea level rise: measuring and modelling cliffline dynamics on the Suffolk Coast, UK. Glob. Planet. Chang. 80-81, 165–179.

Brooks, S.M., Spencer, T., 2014. Importance of decadal scale variability in shoreline response: examples from soft rock cliffs, East Anglian coast, UK. J. Coast. Conserv. 18, 581–593.

Brooks, S.M., Spencer, T., Christie, E.K., 2017. Storm impacts and shoreline recovery: mechanisms and controls in the southern North Sea. Geomorphology 283, 48–60.

Bruun, P., 1954. Coast erosion and the Development of Beach Profiles Beach Erosion Board.

Burningham, H., French, J., 2013. Is the NAO winter index a reliable proxy for wind climate and storminess in Northwest Europe? Int. J. Climatol. 33, 2036–2049.

Burvingt, O., Masselink, G., Scott, T., Davidson, M., Russell, P., 2018. Climate forcing of regionally-coherent extreme storm impact and recovery on embayed beaches. Mar. Geol. 401, 112–128.

Carapuço, M.M., Taborda, R., Silveira, T.M., Psuty, N.P., Andrade, C., Freitas, M.C., 2016. Coastal geoindicators: Towards the establishment of a common framework for sandy coastal environments. Earth Sci. Rev. 154, 183–190.

Castelle, B., Marieu, V., Bujan, S., Splinter, K.D., Robinet, A., Sénéchal, N., Ferreira, S., 2015. Impact of the winter 2013–2014 series of severe Western Europe storms on a double-barred sandy coast: Beach and dune erosion and megacusp embayments. Geomorphology 238, 135–148.

Castelle, B., Dodet, G., Masselink, G., Scott, T., 2017. A new climate index controlling winter wave activity along the Atlantic coast of Europe: the West Europe pressure Anomaly. Geophys. Res. Lett. 44, 1384–1392.

Castelle, B., Dodet, G., Masselink, G., Scott, T., 2018. Increased winter-mean wave height, variability, and periodicity in the Northeast Atlantic over 1949–2017. Geophys. Res. Lett. 45, 3586–3596.

Castelle, B., Bujan, S., Marieu, V., Ferreira, S., 2020. 16 years of topographic surveys of rip-channelled high-energy meso-macrotidal sandy beach. Sci. Data 7, 410.

Christiansen, M., Davidson-Arnott, R., 2004. The effects of dune ramps on sediment supply to coastal foredunes, Skallingen Denmark. Geografisk Tidskrift 104, 29–41.

Coco, G., Senechal, N., Rejas, A., Bryan, K.R., Capo, S., Parisot, J.P., Brown, J.A., Macmahan, J.H.M., 2014. Beach response to a sequence of extreme storms. Geomorphology 204, 493–501.

Cooper, J.A.G., Masselink, G., Coco, G., Short, A.D., Castelle, B., Rogers, K., Anthony, E., Green, A.N., Kelley, J.T., Pilkey, O.H., 2020. Sandy beaches can survive sea-level rise. Nat. Clim. Chang. 10, 993–995.

Costas, S., DE Sousa, L.B., Kombiadou, K., Ferreira, Ó., Plomaritis, T.A., 2020. Exploring foredune growth capacity in a coarse sandy beach. Geomorphology 371, 107435.

Cowell, P.J., Thom, B.G., Jones, R.A., Everts, C.H., Simanovic, D., 2006. Management of uncertainty in predicting climate-change impacts on beaches. J. Coast. Res. 22, 232–245.

Crapoulet, A., Héquette, A., Marin, D., Levoy, F., Bretel, P., 2017. Variations in the response of the dune coast of northern France to major storms as a function of available beach sediment volume. Earth Surf. Process. Landf. 42, 1603–1622.

Davidson-Arnott, R.G.D., Bauer, B.O., 2009. Aeolian sediment transport on a beach: thresholds, intermittency, and high frequency variability. Geomorphology 105, 117–126.

Davidson-Arnott, R.G.D., Bauer, B.O., 2021. Controls on the geomorphic response of beach-dune systems to water level rise. J. Great Lakes Res. 47, 1594–1612.

Dean, R.G., Houston, J.R., 2016. Determining shoreline response to sea level rise. Coast. Eng. 114, 1–8.

Den Heijer, C., Baart, F., Van Koningsveld, M., 2012. Assessment of dune failure along the Dutch coast using a fully probabilistic approach. Geomorphology 143–144, 95–103.

Diamantidou, E., Santinelli, G., Giardino, A., Stronkhorst, J., DE Vries, S., 2020. An automatic procedure for dune foot position detection: application to the Dutch Coast. J. Coast. Res. 36 (668–675), 8.

Dissanayake, P., Brown, J., Wisse, P., Karunarathna, H., 2015. Effects of storm clustering on beach/dune evolution. Mar. Geol. 370, 63–75.

Donker, J., VAN Maarseveen, M., Ruessink, G., 2018. Spatio-Temporal Variations in Foredune Dynamics Determined with Mobile Laser Scanning. J. Mar. Sci. Eng. 6, 126.

Doyle, T.B., Woodroffe, C.D., 2018. The application of LiDAR to investigate foredune morphology and vegetation. Geomorphology 303, 106–121.

Early, C.S., Masselink, G., Russell, P., 2018. The role of beach morphology on coastal cliff erosion under extreme waves. Earth Surf. Process. Landf. 43, 1213–1228.

Fellowes, T.E., Vila-Concejo, A., Gallop, S.L., 2019. Morphometric classification of swell-dominated embayed beaches. Mar. Geol. 411, 78–85.

Ferreira, Ó., 2006. The role of storm groups in the erosion of sandy coasts. Earth Surf. Process. Landf. 31, 1058–1060.

George, D.A., Largier, J.L., Storlazzi, C.D., Barnard, P.L., 2015. Classification of rocky headlands in California with relevance to littoral cell boundary delineation. Mar. Geol. 369, 137–152.

Guisado-Pintado, E., Jackson, D.W.T., 2019. Coastal impact from high-energy events and the importance of concurrent forcing parameters: the cases of storm Ophelia (2017) and storm Hector (2018) in NW Ireland. Front. Earth Sci. 7.

Hird, S., Stokes, C., Masselink, G., 2021. Emergent coastal behaviour results in extreme dune erosion decoupled from hydrodynamic forcing. Mar. Geol. 442, 106667.

Hoonhout, B., de Vries, S., 2017. Field measurements on spatial variations in aeolian sediment availability at the Sand Motor mega nourishment. Aeolian Res. 24, 93–104.

Houser, C., Wernette, P., Rentschlar, E., Jones, H., Hammond, B., Trimble, S., 2015. Post storm beach and dune recovery: implications for barrier island resilience. Geomorphology 234, 54–63.

IPCC, 2021. Climate change 2021: The physical science basis. In: Masson-Delmotte, V., Zhai, P., Pirani, A., Connors, S.L., Péan, C., Berger, S., Caud, N., Chen, Y., Goldfarb, L., Gomis, M.I., Huang, M., Leitzell, K., Lonnoy, E., Matthews, J.B.R., Maycock, T.K., Waterfield, T., Yelekçi, O., Yu, R., Zhou, B. (Eds.), Contribution of Working Group I to the Sixth Assessment Report of the Intergovernmental Panel on Climate Change. Cambridge.

Jackson, Cooper, 1999. Beach fetch distance and aeolian sediment transport. Sedimentology 46, 517–522.

Jackson, D.W.T., Cooper, J.A.G., O'connor, M., Guisado-Pintado, E., Loureiro, C., Anfuso, G., 2016. Field measurements of intertidal bar evolution on a high-energy beach system. Earth Surf. Process. Landf. 41, 1107–1114.

Kandrot, S., Farrell, E., Devoy, R., 2016. The morphological response of foredunes at a breached barrier system to winter 2013/2014 storms on the southwest coast of Ireland. Earth Surf. Process. Landf. 41, 2123–2136.

Karunarathna, H., Pender, D., Ranasinghe, R., Short, A., Reeve, D., 2013. The effects of storm clustering on beach profile variability. Mar. Geol. 348, 103–112.

King, E.V., Conley, D.C., Masselink, G., Leonardi, N., Mccarroll, R.J., Scott, T., Valiente, N.G., 2021. Wave, tide and topographical controls on headland sand bypassing. J. Geophys. Res. Oceans 126, e2020JC017053.

Knutson, T.R., Chung Maya, V., Vecchi, Gabriel, Sun, Jingru, Hsieh, Tsung-Lin, Smith Adam, J.P., 2021. Climate Change is Probably Increasing the Intensity of Tropical Cyclones (Zenodo).

Konstantinou, A., Stokes, C., Masselink, G., Scott, T., 2021. The extreme 2013/14 winter storms: Regional patterns in multi-annual beach recovery. Geomorphology 389, 107828.

Loureiro, C., Cooper, A., 2019. Temporal variability in winter wave conditions and storminess in the northwest of Ireland, 51, 16.

Lozano, I., Devoy, R.J.N., May, W., Andersen, U., 2004. Storminess and vulnerability along the Atlantic coastlines of Europe: analysis of storm records and of a greenhouse gases induced climate scenario. Mar. Geol. 210, 205–225.

Masselink, G., Austin, M., Scott, T., Poate, T., Russell, P., 2014. Role of wave forcing, storms and NAO in outer bar dynamics on a high-energy, macro-tidal beach. Geomorphology 226, 76–93.

Masselink, G., Castelle, B., Scott, T., Dodet, G., Suanez, S., Jackson, D., Floc'h, F., 2016a. Extreme wave activity during 2013/2014 winter and morphological impacts along the Atlantic coast of Europe. Geophys. Res. Lett. 43, 2135–2143.

Masselink, G., Scott, T., Poate, T., Russell, P., Davidson, M., Conley, D., 2016b. The extreme 2013/2014 winter storms: hydrodynamic forcing and coastal response along the southwest coast of England. Earth Surf. Process. Landf. 41, 378–391.

Mccarroll, R.J., Masselink, G., Valiente, N.G., Scott, T., Wiggins, M., Kirby, J.-A., Davidson, M., 2021. A rules-based shoreface translation and sediment budgeting tool for estimating coastal change: ShoreTrans. Mar. Geol. 435, 106466.

Orford, J.D., Carter, R.W.G., 1995. Examination of mesoscale forcing of a swash-aligned, gravel barrier from Nova Scotia. Mar. Geol. 126, 201–211.

Peng, D., Hill, E.M., Meltzner, A.J., Switzer, A.D., 2019. Tide gauge records show that the 18.61-year nodal tidal cycle can change high water levels by up to 30 cm. J. Geophys. Res. Oceans 124, 736–749.

Pollard, J.A., Brooks, S.M., Spencer, T., 2019. Harmonising topographic & remotely sensed datasets, a reference dataset for shoreline and beach change analysis. Sci. Data 6, 42.

Pollard, J.A., Spencer, T., Brooks, S.M., Christie, E.K., Möller, I., 2020. Understanding spatio-temporal barrier dynamics through the use of multiple shoreline proxies. Geomorphology 354, 107058.

Ponte, R.M., Carson, M., Cirano, M., Domingues, C.M., Jevrejeva, S., Marcos, M., Mitchum, G., van de Wal, R.S.W., Woodworth, P.L., Ablain, M., Ardhuin, F., Ballu, V., Becker, M., Benveniste, J., Birol, F., Bradshaw, E., Cazenave, A., De Mey-Frémaux, P., Durand, F., Ezer, T., Fu, L.-L., Fukumori, I., Gordon, K., Gravelle, M., Griffies, S.M., Han, W., Hibbert, A., Hughes, C.W., Idier, D., Kourafalou, V.H., Little, C.M., Matthews, A., Melet, A., Merrifield, M., Meyssignac, B., Minobe, S., Penduff, T., Picot, N., Piecuch, C., Ray, R.D., Rickards, L., Santamaría-Gómez, A., Stammer, D., Staneva, J., Testut, L., Thompson, K., Thompson, P., Vignudelli, S., Williams, J., Williams, S.D.P., Wöppelmann, G., Zanna, L., Zhang, X., 2019. Towards Comprehensive observing and modeling systems for monitoring and predicting regional to coastal sea level. Front. Mar. Sci. 6.

Rogers, M.S.J., Bithell, M., Brooks, S.M., Spencer, T., 2021. VEdge_Detector: automated coastal vegetation edge detection using a convolutional neural network. Int. J. Remote Sens. 42, 4805–4835.

Rosati, J.D., Dean, R.G., Walton, T.L., 2013. The modified Bruun Rule extended for landward transport. Mar. Geol. 340, 71–81.

Ruessink, B.G., Jeuken, M.C.J.L., 2002. Dunefoot dynamics along the Dutch coast. Earth Surf. Process. Landf. 27, 1043–1056.

Ruessink, B.G., Schwarz, C.S., Price, T.D., Donker, J.J.A., 2019. A multi-year data set of beach-foredune topography and environmental forcing conditions at Egmond aan Zee, the Netherlands. Data 73.

Ruz, M.-H., Meur-Ferec, C., 2004. Influence of high water levels on aeolian sand transport: upper beach/dune evolution on a macrotidal coast, Wissant Bay, northern France. Geomorphology 60, 73–87.

Sallenger, A.H., 2000. Storm impact scale for barrier islands. J. Coast. Res. 16, 890–895.

Scott, T., Masselink, G., Russell, P., 2011. Morphodynamic characteristics and classification of beaches in England and Wales. Mar. Geol. 286, 1–20.

Scott, T., Masselink, G., O'hare, T., Saulter, A., Poate, T., Russell, P., Davidson, M., Conley, D., 2016. The extreme 2013/2014 winter storms: beach recovery along the southwest coast of England. Mar. Geol. 382, 224–241.

Sherman, D.J., Li, B., 2012. Predicting aeolian sand transport rates: a reevaluation of models. Aeolian Res. 3, 371–378.

Smith, A., Houser, C., Lehner, J., George, E., Lunardi, B., 2020. Crowd-sourced identification of the beach-dune interface. Geomorphology 367, 107321.

Spencer, T., Brooks, S.M., Evans, B.R., Tempest, J.A., Möller, I., 2015. Southern North Sea storm surge event of 5 December 2013: Water levels, waves and coastal impacts. Earth Sci. Rev. 146, 120–145.

Stockdon, H.F., Holman, R.A., Howd, P.A., Sallenger, A.H., 2006. Empirical parameterization of setup, swash, and runup. Coast. Eng. 53, 573–588.

Turner, I.L., Harley, M.D., Short, A.D., Simmons, J.A., Bracs, M.A., Phillips, M.S., Splinter, K.D., 2016. A multi-decade dataset of monthly beach profile surveys and inshore wave forcing at Narrabeen, Australia. Sci. Data 3, 160024.

Valiente, N.G., Masselink, G., Scott, T., Conley, D., Mccarroll, R.J., 2019. Role of waves and tides on depth of closure and potential for headland bypassing. Mar. Geol. 407, 60–75.

van Ijzendoorn, C.O., DE Vries, S., Hallin, C., Hesp, P.A., 2021. Sea level rise outpaced by vertical dune toe translation on prograding coasts. Sci. Rep. 11, 12792.

Vitousek, S., Barnard, P.L., Limber, P., Erikson, L., Cole, B., 2017. A model integrating longshore and cross-shore processes for predicting long-term shoreline response to climate change. J. Geophys. Res. Earth Surf. 122, 782–806.

Vos, K., Splinter, K.D., Harley, M.D., Simmons, J.A., Turner, I.L., 2019. CoastSat: a Google Earth Engine-enabled Python toolkit to extract shorelines from publicly available satellite imagery. Environ. Model. Softw. 122, 104528.

Vousdoukas, M.I., Almeida, L.P.M., Ferreira, Ó., 2012. Beach erosion and recovery during consecutive storms at a steep-sloping, meso-tidal beach. Earth Surf. Process. Landf. 37, 583–593.

Vousdoukas, M.I., Ranasinghe, R., Mentaschi, L., Plomaritis, T.A., Athanasiou, P., Luijendijk, A., Feyen, L., 2020. Sandy coastlines under threat of erosion. Nat. Clim. Chang. 10, 260–263.

Vries, S.D., Harley, M.D., Schipper, M.A.D., Ruessink, G., 2015. Dune growth due to Aeolian sediment transport and the role of the beach and intertidal zone. Coast. Sedim. 2015.

WCRP, 2018. Global sea-level budget 1993–present. Earth Syst. Sci. Data 10, 1551–1590.

Wernette, P., Houser, C., Bishop, M.P., 2016. An automated approach for extracting Barrier Island morphology from digital elevation models. Geomorphology 262, 1–7.

Wiggins, M., Scott, T., Masselink, G., Russell, P., Mccarroll, R.J., 2019. Coastal embayment rotation: response to extreme events and climate control, using full embayment surveys. Geomorphology 327, 385–403.